PAPER

Modulation of oxygen vacancies assisted ferroelectric and photovoltaic properties of (Nd, V) co-doped BiFeO$_3$ thin films

To cite this article: Radhe Agarwal *et al* 2018 *J. Phys. D: Appl. Phys.* **51** 275303

View the article online for updates and enhancements.

Modulation of oxygen vacancies assisted ferroelectric and photovoltaic properties of (Nd, V) co-doped BiFeO$_3$ thin films

Radhe Agarwal[1] , **Yogesh Sharma**[1,2] , **Seungbum Hong**[2,3]
and Ram S Katiyar[1]

[1] Department of Physics, University of Puerto Rico, San Juan, PR 00931, United States of America
[2] Material Science Division, Argonne National Laboratory, Lemont, IL 60439, United States of America
[3] Department of Materials Science and Engineering, KAIST, Daejeon 34141, Republic of Korea

E-mail: yks181086@gmail.com and seungbum@kaist.ac.kr

Abstract

We are reporting on the improved ferroelectric and photovoltaic properties of (Nd^{3+}, V^{5+}) co-doped (Bi$_{0.95}$Nd$_{0.05}$)(Fe$_{1-x}$V$_x$)O$_3$ (BNFVO) ($x = 0.01, 0.03$) thin films grown by PLD. BNFVO thin films showed reduced leakage current, lower optical bandgap, and improved ferroelectricity compared to BFO films, which can be explained by valance change and extinguishing oxygen vacancies due to the doping effect. Piezoresponse force microscopy measurements showed an improved domain back switching in doped thin films indicating that the suppression of oxygen vacancies offset the effect of polarization flipping caused by doping. Further, we found a relatively stable and enhanced photovoltaic effect in BNFVO films with an order of magnitude higher photocurrent and almost doubled photovoltage in comparison to BFO films, which can be explained by less recombination between hopping electrons and oxygen vacancies. Our results demonstrate the significance of dopant selection to suppress the oxygen vacancies for improved ferroelectric and photovoltaic properties of BFO films.

Keywords: ferroelectric, bismuth ferrite, photovoltaic, oxygen vacancies, chemical doping

S Supplementary material for this article is available online

(Some figures may appear in colour only in the online journal)

1. Introduction

Multiferroics are the materials which possess the relatively uncommon and rare combination of at least two of the following properties: ferroelectricity, ferroelasticity, and ferromagnetism. It is even rarer to find materials with the unique simultaneous occurrence of ferroelectricity and ferromagnetism at room temperature. Such types of multiferroics offer the potential to control both ferroic orderings, i.e. ferroelectric polarization and magnetism together [1–5]. Very few materials satisfy these criteria. BiFeO$_3$ (BFO) can be referred as one of the most studied room temperature multiferroics [6–9] because of its distinct physical properties. BFO shows a rhombohedral distorted perovskite structure (ABO$_3$) at room temperature. The low symmetry distorted structure in BFO occurs due to the B-cation shift from an ideal perovskite (ABO$_3$) lattice because of electron-orbital interaction between center cation and the surrounding oxygens [10, 11]. Fortunately, noncentrosymmetry arises from the structural distortions which can advance the functionalities of the material as with BFO, which shows room temperature multiferroicity with large spontaneous polarization (90 μC cm^{-2}) and weak ferromagnetism [7–9, 12]. Also, BFO shows lower optical bandgap (2.67 eV) compared to other wide band-gap
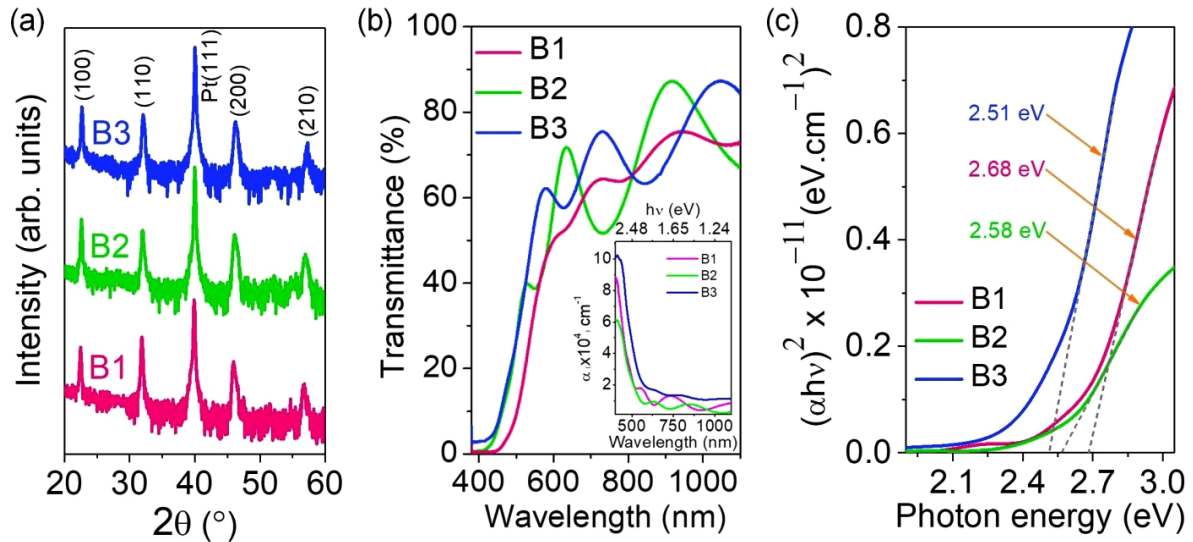
Figure 1. (a) XRD patterns of 150 nm thick undoped (B1) and doped (B2 and B3) BFO films on Pt/Si substrate. (b) Optical transmittance of B1, B2, and B3 film of the same thickness (150 nm) deposited on quartz substrate. Inset shows the absorption coefficient (α) as a function of photon energy ($h\nu$), which was used to determine bandgap using Tauc plot fitting. (c) $(\alpha h\nu)^2$ versus $h\nu$ plot showing the varying bandgap corresponding to vanadium doping concentration.

perovskite materials (BaTiO$_3$, LiNbO$_3$ and Pb(Zr,Ti)O$_3$), which makes it suitable for advanced optoelectronic and photovoltaic applications [13, 14].

Despite showing excellent multiferroic and photovoltaic properties, there are remaining challenges in implementing BFO into devices, such as high leakage current and large coercive field. The origin of high leakage current in BFO can be attributed to the presence of secondary phases, charge defects, and oxygen vacancies [15, 16]. In BFO, oxygen vacancies can misleadingly affect the magnitude, stability, and polarity of photovoltaic properties in ferroelectric films [17–19]. An unstable photovoltaic behavior can be observed due to the presence of oxygen vacancies along with a negative impact on ferroelectric properties such as fatigue and domain pinning [18]. There have been many attempts to quench charge defects and oxygen vacancies by manipulating chemically-induced lattice strain using suitable dopants. Another approach to control oxygen vacancies is via interface engineering by inserting an insulating layer at metal/BFO/metal interfaces [20] or by introducing an insulating layer between two BFO nanolaminates [21]. To control bulk oxygen vacancies, an appropriate choice of dopant is critical, which can homogenize charge and spin ordering while enhancing ferroelectricity and magnetism simultaneously. An aliovalent ion doping at Fe-site promotes the stable valance state of Fe in BFO (i.e. Fe^{3+}) which can substantially suppress the oxygen vacancies [22–24]. Also, isovalent doping at Bi-site helps to bring down the volatility of Bi which can eliminate the Bi associated oxygen vacancies [25].

In this paper, an attempt has been made to improve ferroelectric and photovoltaic properties via chemical doping in BFO thin films grown by pulsed laser deposition (PLD). We observed that doped (Bi$_{0.95}$Nd$_{0.05}$)(Fe$_{1-x}$V$_x$)O$_3$ thin films showed significant reduction in leakage current, enhanced

ferroelectricity, and improved photovoltaic properties compared to undoped BFO films. Our results can be explained by the dopant induced valance effect and reduced oxygen vacancies at different doping concentrations.

2. Experimental

BFO thin films were deposited onto Pt/TiO$_2$/SiO$_2$/Si substrates PLD. A conventional cleaning process using de-ionized water, acetone, and isopropanol was applied to clean Pt/TiO$_2$/SiO$_2$/Si substrates. A KrF excimer laser ($\lambda = 248$ nm) operating at 5 Hz was used for target ablation. The laser fluence was 1.8 J cm^{-2} with a spot area of 3.8 mm^2 on the target. The target-substrate distance was set at 5 cm. The deposition was performed under oxygen partial pressure of 80 mTorr at substrate temperature of 690 °C. After deposition, the films were cooled to room temperature at 15 °C min^{-1} while maintaining the same oxygen partial pressure throughout the cooling time. For optical measurements, B1, B2 and B3 films were deposited onto optical grade quartz (two sides polished (0 0 1)) following the same deposition conditions. Film thicknesses were measured using mechanical profilometer (Veeco) while creating a sharp step on the films during the growth. Five data sets were used for averaging the thickness. Phase pure BiFeO$_3$ (BFO, B1) and (Bi$_{0.95}$Nd$_{0.05}$)(Fe$_{1-x}$V$_x$)O$_3$ (x = 0.01; B2, and x = 0.03; B3) ceramic targets were synthesized by a conventional solid-state reaction method using Bi$_2$O$_3$, Fe$_2$O$_3$, Nd$_2$O$_3$ and V$_2$O$_5$ powder precursors (Alfa-Aesar >99.9%). All the powders were weighed in stoichiometric amounts according to different target compositions followed by mixing in ball milling for up to 6 h. It is noted that an excess amount of Bi$_2$O$_3$ was used (5 weight % for BFO and 4.5 weight % for (Bi$_{0.95}$Nd$_{0.05}$)(Fe$_{1-x}$V$_x$)O$_3$) to compensate for Bi-volatility during preparation. These powder mixtures were calcined

at furnace temperature of 800 °C in air for 1.5 h. After calcination, these powders were pressed into pellets using a cold isostatic method (~30 MPa) and sintered at 820 °C in air for 1 h to form polycrystalline ceramic targets. Phase purity and compositional uniformity of these targets were confirmed using x-ray diffraction (XRD) (see supplementary information file, figure S1, available online at stacks.iop.org/JPhysD/51/275303/mmedia) and transmission electron microscopy equipped with energy dispersive x-ray spectroscopy (see supplementary information file, figures S2–S4). A dc-magnetron sputtering was used to deposit 50 nm thick Pt square electrodes onto the films using a shadow square mask of the area of 80 × 80 μm^2.

Crystalline structure of the films was studied using the XRD technique (Rigaku D/Max Ultima III with a CuKα source of wavelength λ = 1.5405 Å) operated at a scan rate of 0.5° min^{-1} over the angular range (2θ) between 20 and 80°. Plan-view SEM image and SEM-EDS elemental maps were recorded to check elemental composition of as-grown B3 thin films (see supplementary information file, figure S5). Chemical compositions of as-deposited films were analyzed using x-ray photoelectron spectroscopy (XPS). XPS measurements were performed on pristine B1 and B3 films to investigate the chemical states of the films. Binding energy corresponding to C 1s peak was utilized to correct the energy shift of Fe 2p and V 2p core levels to account for the x-ray induced insulator charging that otherwise could have caused a systematic experimental error. Optical transmittance characteristics were measured by UV–Vis spectrometer. Ferroelectric domain switching and local piezoelectric responses were analyzed by piezoresponse force microscopy (PFM) mode using a commercial atomic force microscope (AFM) (Asylum Research, MFP-3D). An ac modulation voltage of 1 V (peak to peak), drive frequencies of 338 kHz, and a scan frequency of 1 Hz were used during PFM measurements. Macroscopic ferroelectric properties were characterized using RT6000 loop tester (Radiant Technologies). Photovoltaic measurements were performed using a Keithley-2401 electrometer under 1 sun AM 1.5 solar simulator with light source density ~1 kW m^{-2}.

3. Results and discussion

Figure 1(a) shows XRD patterns of B1, B2 and B3 thin films deposited on Pt/TiO$_2$/SiO$_2$/Si substrate. XRD results reveal single phase polycrystalline growth of our thin films with rhombohedral (R3c) symmetry [26]. To study the optical properties, we have measured optical transmittance spectra of single phase B1, B2 and B3 thin films deposited on optical quality quartz substrates shown in figure 1(b). Based on the transmittance characteristics of the films, figure 1(c) represents the estimated direct band gap calculated by the linear extrapolation of $(\alpha h\nu)^2$ versus $h\nu$ plot to the x-axis where the absorption coefficient (α) becomes zero [27, 28]. The inset of figure 1(b) shows the spectral dependence of absorption coefficient (α). We observed that addition of dopants caused absorption peak to shift towards lower photon energy, which
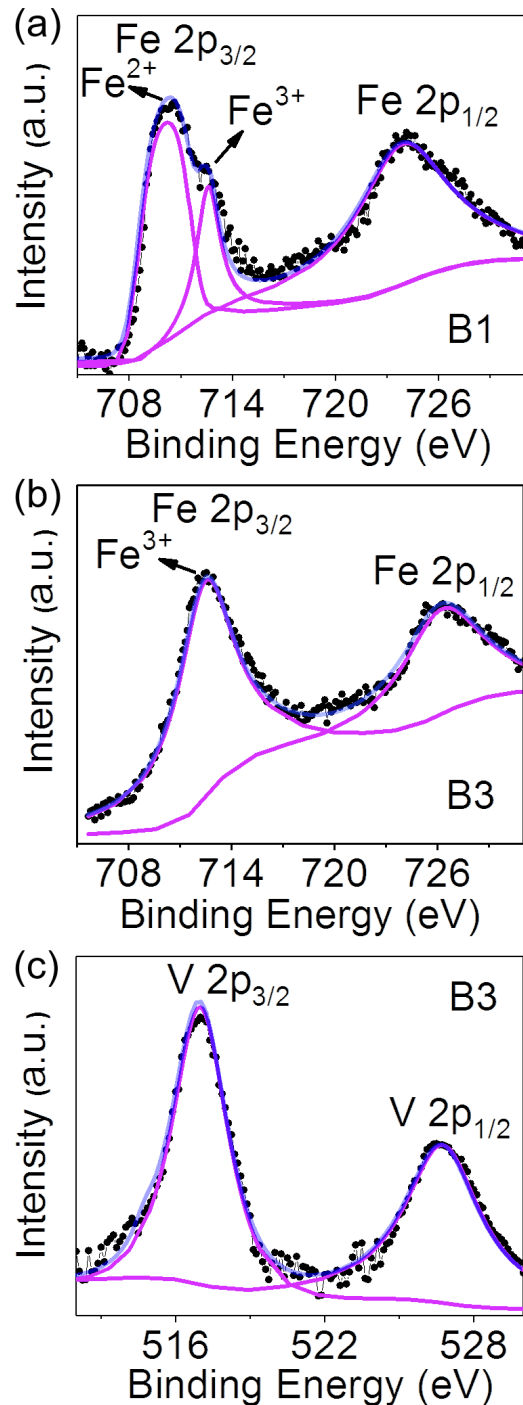

Figure 2. XPS spectra of Fe 2p orbital in; (a) B1 film where Fe 2p$_{3/2}$ peak can be fitted in a combination of Fe^{2+} and Fe^{3+} valance states, and (b) B3 film where Fe 2p$_{3/2}$ peak shows only the presence of Fe^{3+} valance state of Fe. (c) XPS spectrum of V 2p orbital in B3 film.

can enhance absorption capability of the doped BFO thin films. Such optical modulation in doped films can be an effect of interplay between the varying concentrations of doping and oxygen vacancies [29].

To get further insight into modification in charge defects via vanadium (V) doping, we studied the XPS spectra of Fe and V ions on the surface of B1 and B3 films, as shown in
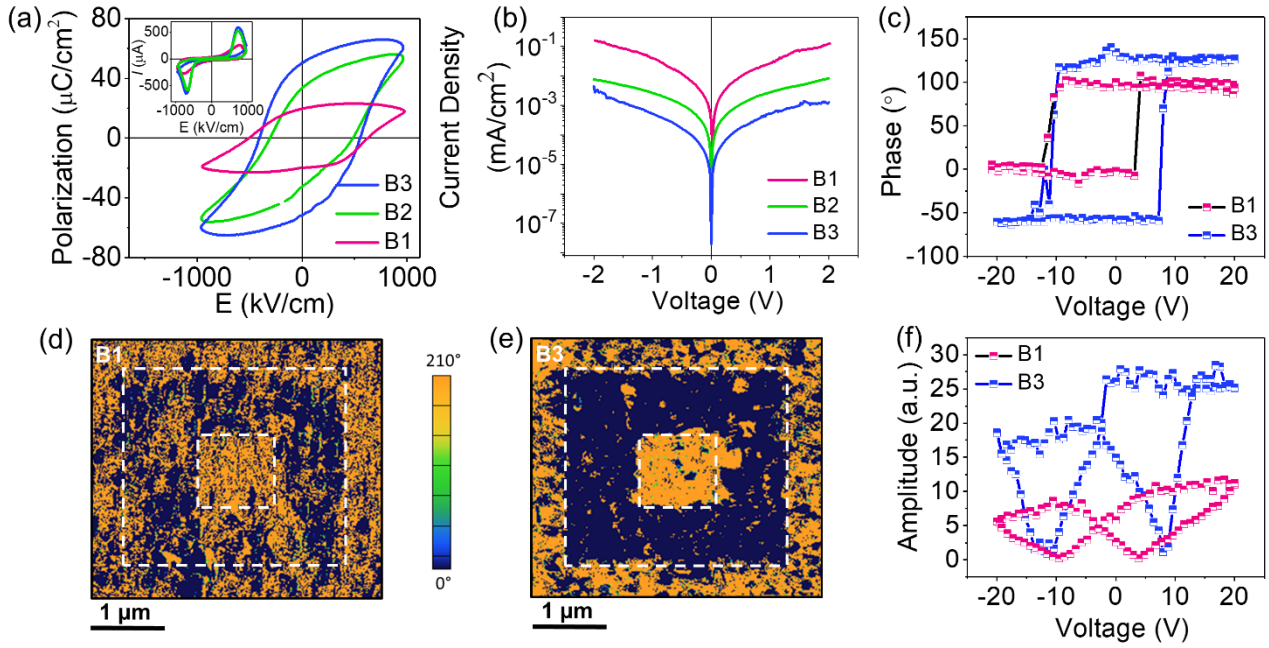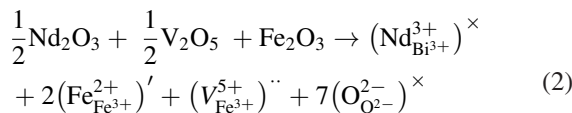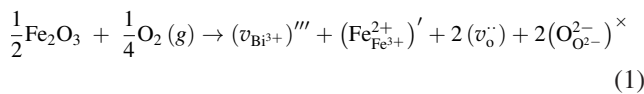
J. Phys. D: Appl. Phys. **51** (2018) 275303

R Agarwal *et al*

Figure 3. (a) Room temperature P–E loop measured at $f = 1$ kHz. Inset shows the corresponding polarization switching currents. (b) Leakage current measurements on B1, B2, and B3 films. (d) and (e) room temperature out-of-plane PFM images of ± 12 V tip-bias written domain patterns onto B1 and B3 films. (c) Phase, and (f) amplitude hysteresis loops of B1 and B3 films.

figure 2. XPS spectra of Bi and Nd have been included in the supplementary information file (figure S6). Figure 2(a) confirms the multivalent states of Fe (i.e. $Fe^{2+/3+}$) in B1 thin film, where the Fe $2p_{3/2}$ and Fe $2p_{1/2}$ core-level peaks become broader and shift to comparatively lower binding energies, indicating a reduction of the oxidation state from 3+ to 2+ [13, 24, 30]. The Fe $2p_{3/2}$ peak in B1 film was deconvoluted into two peaks corresponding to Fe^{3+} (~712.61 eV) and Fe^{2+} (~710.22 eV) states. Therefore, in B1 film, the Fe ion shows a mixture of 3+ and 2+ oxidation states. This indicates that B1 film is reduced, having defects in the form of oxygen vacancies to balance the charges. However, in the case of B3 film, the Fe $2p_{3/2}$ peak did not show unusual shoulder peak or broadening and can be fitted by a single peak corresponding to Fe^{3+} (~712.63 eV), indicating that film is not reduced in comparison to B1 film.

Moreover, we observed that XPS spectra of V did not show any signature of reduced bonding signal as the two peaks corresponding to V $2p_{3/2}$ and $2p_{1/2}$ were found to be located at ~517.18 and ~526.31 eV, respectively, with a separation of ~9.13 eV, which indicates that vanadium dominantly exists in the form of V^{5+} in our doped BFO samples [31, 32]. Substitution of Fe^{3+} with higher valance ion V^{5+} in doped films would lead to suppression of oxygen vacancies [13], explained by the requirement of charge neutrality based on the following defect equations (1) and (2);

$$\frac{1}{2}Fe_2O_3 + \frac{1}{4}O_2(g) \rightarrow (v_{Bi^{3+}})''' + (Fe_{Fe^{3+}}^{2+})' + 2(v_o^{\cdot\cdot}) + 2(O_{O^{2-}}^{2-})^\times \tag{1}$$

$$\frac{1}{2}Nd_2O_3 + \frac{1}{2}V_2O_5 + Fe_2O_3 \rightarrow (Nd_{Bi^{3+}}^{3+})^\times$$
$$+ 2(Fe_{Fe^{3+}}^{2+})' + (V_{Fe^{3+}}^{5+})^{\cdot\cdot} + 7(O_{O^{2-}}^{2-})^\times \tag{2}$$

where $v_o^{\cdot\cdot}$ denotes an oxygen vacancy. Therefore, the oxygen vacancies can be suppressed by the high valence V ions. In addition, neodymium (Nd) doping can overcome the Bi volatility which can further eliminate oxygen vacancies in the films [30, 33].

In oxide ferroelectrics, it has been reported that the suppression of chemical defects can reduce the leakage current contribution and thus improve the ferroelectric properties [15, 16]. Based on XPS results, we believe that our doped thin films can show improved ferroelectricity compared to the undoped films. To confirm this, room temperature polarization versus electric field (P–E) loops were measured for B1, B2 and B3 thin film capacitors at 1 kHz, as shown in figure 3(a). We observed nearly rectangular and saturated loops for these capacitors, where the remnant polarization was measured as high as ~55 μC cm^{-2} for B3 compared to ~23 μC cm^{-2} for B1 capacitor. We also observed a slight decrease in the coercive field for B3 as compared to undoped B1 capacitor [34, 35]. Inset of figure 3(a) shows the improvement in polarization switching current response with doping, which can be attributed to true macroscopic ferroelectric response in our doped films [36, 37]. Such consistent improvements in ferroelectric properties after an increase in doping concentration can be explained by valance effect and reduction in concentration of oxygen vacancies due to doping [22–25, 38]. Moreover, doping-induced suppression of oxygen vacancies also promoted low leakage currents in B2 and B3 samples as compared to undoped B1, as shown in figure 3(b).

The nanoscale ferroelectric properties of our thin films were studied using PFM. The upward and downward polarizations were successively written by the conducting PFM-tip bias of -12 V and $+12$ V in 3×3 μm^2 and 1×1 μm^2 areas of B1 and B3 films. After writing, the out-of-plane PFM reading

J. Phys. D: Appl. Phys. **51** (2018) 275303
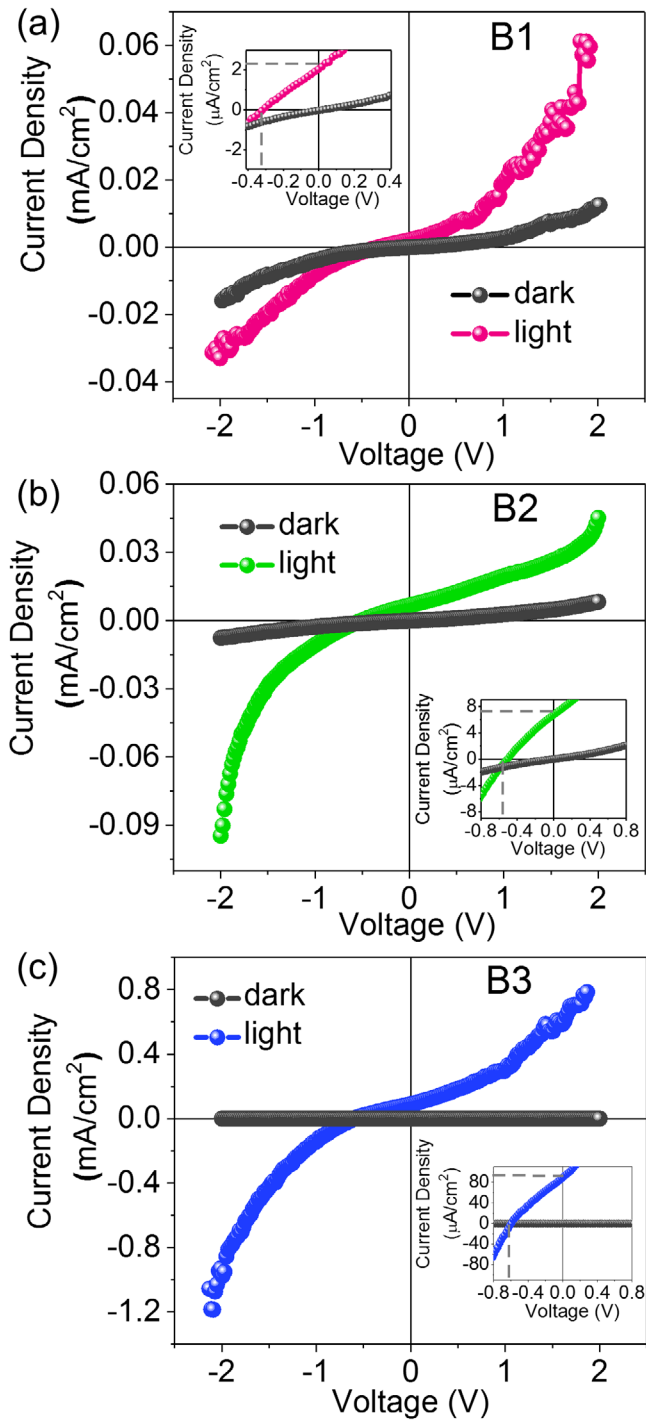
R Agarwal *et al*

Figure 4. Room temperature current density versus voltage characteristics in dark and under white light illumination for (a) B1, (b) B2, and (c) B3 films in unpoled state. Inset shows an enlarged view indicating photocurrents and photovoltages.

Table 1. Photovoltaic performance parameters from *J–V* data measured on B1, B2 and B3 thin film.

Sample	V_{OC} (V)	J_{SC} (μA cm^{-2})	FF	η (%)
B1	(−)0.32	2.4	0.28	0.002
B2	(−)0.58	7.6	0.30	0.01
B3	(−)0.65	98.5	0.31	0.2

loops, as shown in figures 3(c) and (f). The characteristic butterfly loops were observed in amplitude signals of these films, where the phase loops indicate a clear switching behavior. The collective piezo-response hysteresis loops of B1 and B3 samples also confirm that a clear and complete polarization switching can be accomplished in B3 sample when compared to B1.

We have also investigated the ferroelectric photovoltaic effect in our thin films. Current density versus voltage characteristics were measured on B1, B2 and B3 thin film capacitors in dark and under white light illumination, as shown in figure 4. B2 and B3 films were observed to show enhanced photovoltaic (PV) response as compared to B1. The chemical doping effect on photovoltaic behavior in our BFO films can be seen in terms of more than an order increase in photocurrent density (J_{SC}) and almost double photovoltage (V_{OC}) in B3 film as compared to B1. Table 1 shows a comparison between J_{SC}, V_{OC}, fill factor (FF) and power conversion efficiency (η) values for B1, B2 and B3 thin films. Our calculated fill factor (FF) values are between 0.28–031 which is smaller than the ideal value of 0.7 FF. It has been reported that the FF can be affected by various factors, including carrier mobility, carrier recombination rates, carrier movement due to internal electric field, and contact resistance to the electrodes, etc [39, 40]. However, our power conversion efficiency values are fairly matched with the previous reports on polycrystalline BiFeO$_3$ [41, 42], where B3 thin films shows 100 times larger PV response in comparison to B1. The time dependent behavior of J_{SC} and V_{OC} was also recorded under several on/off light illumination cycles, as shown in figure 5. We observed unstable variations in J_{SC} over time in B1 and B2 samples, where the J_{SC} value was found to continuously increase with time under light illumination. In contrast, the variations in J_{SC} and V_{OC} were found to be comparatively stable in B3 film. Based on previous studies, deterioration in PV response of BFO can be strongly associated with the migration of oxygen vacancies, and the photoresponse can be improved due to less recombination between hopping electrons and oxygen vacancies in stochiometric samples [17, 19, 27, 43]. Therefore, the role of oxygen vacancy is evident to explain the improved PV behavior in our BFO thin films.

4. Conclusions

In summary, we have shown oxygen vacancies in BFO can be reduced by aliovalent ion doping with varying doping concentrations. The oxygen vacancies can be responsible for significant lowering in band gap, possibly due to the orbital reconstruction.
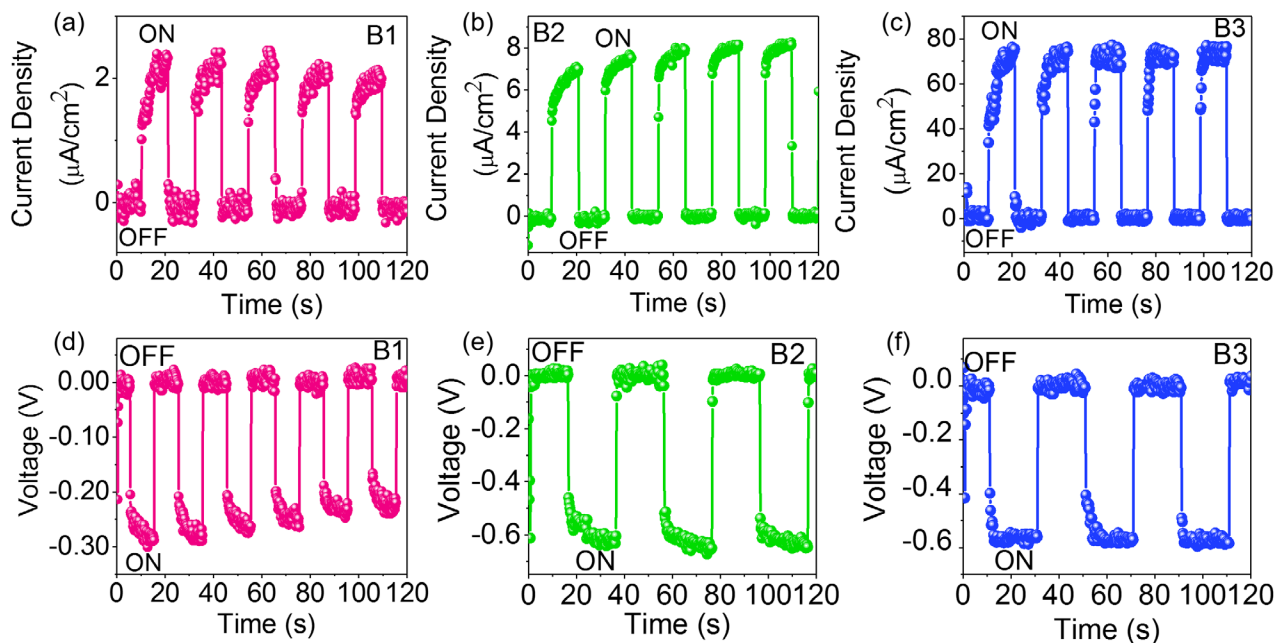
images were acquired in 4 × 4 μm^2 area with an ac voltage of 1 V at 338 kHz, as shown in figures 3(d) and (e). PFM images indicate that the domain back switching is more evident in the B3 sample when compared to B1, which can be explained by the dominance of polarization flipping over oxygen vacancies [27]. Moreover, the local ferroelectric switching behavior of B1 and B3 films was further confirmed by PFM spectroscopy measurement generating phase and amplitude hysteresis

J. Phys. D: Appl. Phys. **51** (2018) 275303

R Agarwal *et al*

Figure 5. Time dependent (a)–(c) photocurrent (J_{SC}) and (d)–(f) photovoltage (V_{OC}) of unpoled B1, B2, and B3 films with light on and off cycles of 20 s duration.

We observed improved ferroelectric behavior and stable photovoltaic responses in doped $Bi_{0.9}Nd_{0.1}Fe_{1-x}V_xO_3$ thin films compared to undoped BFO, which can be explained by valance effect and extinguishing oxygen vacancies due to co-doping. Our results indicate the critical role of oxygen vacancies determining the optical, ferroelectric, and photovoltaic properties and thus demonstrate the significance of dopants selection to quench the oxygen vacancies for improved ferroelectric and photovoltaic behavior in BFO films.

ORCID iDs

Radhe Agarwal https://orcid.org/0000-0002-8944-9423
Yogesh Sharma https://orcid.org/0000-0001-8532-4036
Seungbum Hong https://orcid.org/0000-0002-2667-1983

References

[1] Michel C, Moreau J-M, Achenbach G D, Gerson R and James W J 1969 *Solid State Commun.* **7** 701
[2] Wang J *et al* 2003 *Science* **299** 1719
[3] Yang C H *et al* 2009 *Nat. Mater.* **8** 485
[4] Yang S Y *et al* 2009 *Appl. Phys. Lett.* **95** 062909
[5] Jiang A Q, Wang C, Jin K J, Liu X B, Scott J F, Hwang C S, Tang T A, Lu H B and Yang G Z 2011 *Adv. Mater.* **23** 1277
[6] Choi T, Lee S, Choi Y, Kiryukhin V and Cheong S 2009 *Science* **324** 63
[7] Ji W, Yao K and Liang Y 2010 *Adv. Mater.* **22** 1763
[8] Yi H T, Choi T, Choi S G, Oh Y S and Cheong S-W 2011 *Adv. Mater.* **23** 3403
[9] Yang S Y *et al* 2010 *Nat. Nanotechnol.* **5** 143
[10] Kubel F and Schmid H 1990 *Acta Crystallogr.* B **B46** 698
[11] Neaton J B, Ederer C, Waghmare U V, Spaldin N A and Rabe K M 2005 *Phys. Rev.* B **71** 014113
[12] Seidel J, Fu D, Yang S Y, Alarc O L, Wu J, Ramesh R and Ager J W III 2011 *Phys. Rev. Lett.* **107** 126805
[13] Basu S R, Martin L W, Chu Y-H, Gajek M, Ramesh R, Rai R C, Xu X and Musfeldt J L 2008 *Appl. Phys. Lett.* **92** 091905
[14] Hauser A J, Zhang J, Mier L, Ricciardo R A, Woodward P M, Gustafson T L, Brillson L J and Yang F Y 2008 *Appl. Phys. Lett.* **92** 222901
[15] Valant M, Axelsson A-K and Alford N 2007 *Chem. Mater.* **19** 5431
[16] Yuan G L, Or S W, Wang Y P, Liu Z G and Liu J M 2006 *Solid State Commun.* **138** 76
[17] Gao R L, Yang H W, Chen Y S, Sun J R, Zhao Y G and Shen B G 2014 *Appl. Phys. Lett.* **104** 031906
[18] Guo Y, Guo B, Dong W, Li H and Liu H 2013 *Nanotechnology* **24** 275201
[19] Moubah R, Rousseau O, Colson D, Artemenko A, Maglione M and Viret M 2012 *Adv. Funct. Mater.* **22** 4814

J. Phys. D: Appl. Phys. **51** (2018) 275303

R Agarwal *et al*

[20] Jiang A Q, Lee H J, Kim G H and Hwang C S 2009 *Adv. Mater.* **21** 2870

[21] Lee G, Fernandez E M A, Lian G, Katiyar R S and Auciello O 2015 *Appl. Phys. Lett.* **106** 022905

[22] Maksymovych P, Jesse S, Yu P, Ramesh R, Baddorf A and Kalinin S 2009 *Science* **324** 1421

[23] Katiyar R K, Sharma Y, Barrionuevo D, Kooriyattil S, Pavunny S P, Young J S, Morell G, Weiner B R, Katiyar R S and Scott J F 2015 *Appl. Phys. Lett.* **106** 082903

[24] Sharma Y, Martinez R, Agarwal R, Barrionuevo D, Katiyar R K, Kumar A and Katiyar R S 2016 *J. Appl. Phys.* **120** 194101

[25] Shirolkar M M, Hao C, Dong X, Guo T, Zhang L, Li M and Wang H 2014 *Nanoscale* **6** 4735

[26] Kharel P, Talebi S, Ramachandran B, Dixit A, Naik V M, Sahana M B, Sudakar C, Naik R, Rao M S R and Lawes G 2009 *J. Phys.: Condens. Matter* **21** 036001

[27] Agarwal R, Sharma Y and Katiyar R S 2015 *Appl. Phys. Lett.* **107** 162904

[28] Katiyar R K, Sharma Y, Barrionuevo D, Misra P, Kooriyattil S, Pavunny S P, Morell G, Weiner B R, Scott J F and Katiyar R S 2015 *AIP Adv.* **5** 037109

[29] Lee W-M, Sung J H, Chu K, Moya X, Lee D, Kim C-J, Mathur N D, Cheong S-W, Yang C-H and Jo M-H 2012 *Adv. Mater.* **24** OP49–OP53

[30] Li Y, Fang X and Cao M 2016 *Sci. Rep.* **6** 24837

[31] Sawatzky G A and Post D 1979 *Phys. Rev.* B **20** 1546

[32] Mendialdua J, Casanova R and Barbaux Y 1995 *J. Electron. Spectrosc. Relat. Phenom.* **71** 249–61

[33] Hu Z, Li M, Yu B, Pei L, Liu J, Wang J and Zhao X 2009 *J. Phys. D: Appl. Phys.* **42** 185010

[34] Qi X, Dho J, Tomov R, Blamire M G and Driscoll J L M 2005 *Appl. Phys. Lett.* **86** 062903

[35] Wang Y and Nan C-W 2006 *Appl. Phys. Lett.* **89** 052903

[36] Zhang S, Wang L, Chen Y, Wang D, Yao Y and Ma Y 2012 *J. Appl. Phys.* **111** 074105

[37] Agarwal R *et al* 2018 *Phys. Rev.* B **97** 054109

[38] Wu H *et al* 2013 *J. Phys. D: Appl. Phys.* **46** 145001

[39] Green M 1982 *Solar Cells-Operating Principles, Technology and System Application* (Englewood Cliffs, NJ: Prentice Hall)

[40] Chakrabartty J, Nechache R, Harnagea C, Li S and Rosei F 2016 *Nanotechnology* **27** 215402

[41] Chen B, Li M, Liu Y, Zuo Z, Zhuge F, Zhan Q-F and Li R-W 2011 *Nanotechnology* **22** 195201

[42] Fan Z, Yao K and Wang J 2014 *Appl. Phys. Lett.* **105** 162903

[43] Sharma Y, Misra P, Katiyar R K and Katiyar R S 2014 *J. Phys. D: Appl. Phys.* **47** 425303